Inelastic electron transport through mesoscopic systems: Heating versus cooling and sequential tunneling versus cotunneling processes

Feng Jiang,[1] Jinshuang Jin,[2] Shikuan Wang,[1] and YiJing Yan[1,3,*]

[1]*Department of Chemistry, Hong Kong University of Science and Technology, Kowloon, Hong Kong*

[2]*Department of Physics, Hangzhou Normal University, Hangzhou 310036, China*

[3]*Hefei National Laboratory for Physical Sciences at the Microscale, University of Science and Technology of China, Hefei, Anhui 230026, China*

(Received 18 March 2012; published 14 June 2012)

Inelastic electron transport in quantum dot systems is studied via the hierarchical equations of motion combining a small polaron transformation approach, with differential conductance $dI/dV \sim V$ characteristics being evaluated accurately at the cotunneling level. We observe (i) the *peak* feature of phonon emission Franck-Condon sidebands to the zero-phonon peaks of both polaron and bipolaron in sequential electron transport; (ii) phonon absorption peaks occurring if the phonon temperature is sufficiently higher than that of the carrier electron; and (iii) the *step* feature of Raman sidebands in the cotunneling transport regime. We also evaluate the polaron transport response to a continuous-wave irradiation that induces bias-voltage oscillation. We observe, consistent with experimental results, that (iv) the photon-phonon-assisted tunneling enhances phonon absorptions while suppressing emissions. As the phonon absorption (emission) is associated with the process of absorbing (emitting) energy from (to) the phonon environment, an alternating or tailored field applied to contacts could be a practical means of cooling the mesoscopic quantum-transport device.

DOI: 10.1103/PhysRevB.85.245427 PACS number(s): 72.10.−d, 72.10.Bg, 72.10.Di

I. INTRODUCTION

The interplay between inelasticity and coherence in quantum transport is closely related to the performance of molecular electronics.[1–9] Inelasticity arises intrinsically from the electron-phonon (e-ph) coupling. It is closely related to local heating of the junction, although current-induced cooling could also occur under certain conditions.[10,11] The problem of heating accompanying the electron transport can become quite serious along the miniaturization of devices. It may affect the stability of the device, ultimately resulting in device malfunctioning. At low temperatures, typically below 10 K, the vibrational motion of molecules or lattice environments is almost frozen. However, when electronic current passes through molecules, the molecular lattice motion can be excited by transport electrons, provided that they carry sufficient energy. The probability for such inelastic scattering events depends on the energy of transport electrons controlled by the applied bias. Furthermore, if the tunneling electron resides for sufficiently long time on the molecule, a vibronic state (a localized polaron) may be formed, where the charge influences the nuclear geometry of the molecule. The probability of forming this quasiparticle state depends also on the detailed balance between the transport electronic energy, its dissipation, and vibrational relaxation.[12] In other words, inelasticity or e-ph coupling in quantum transport can lead to rich phenomena such as conformational changes, induced chemical reactions, and electromigration.[13,14] It manifests nonlinearities in the current-voltage curves, which reflect the underlying molecular structure. The method of detecting vibronic signatures in bias spectroscopy is commonly referred to as inelastic tunneling spectroscopy.[15,16]

There are many efforts on understanding the nature of phonon-assisted tunneling.[17–24] The theoretical studies of inelastic quantum transport cover both single-particle and many-particle approaches. The former includes Landauer-Büttiker scattering theory[25] and nonequilibrium Green's function,[26] which can easily deal with large systems, but it is difficult to exploit the essential physics beyond the mean-field treatment in strong Coulomb interaction regime. Many-particle approaches include master equation[27–32] and the real-time diagrammatic technique.[33–36] The master equation approach is perturbative in nature, treating the system-environment coupling at a second-order level. In other words, it treats only sequential tunneling and is not enough in the case of low temperature and strong system-environment coupling. The real-time diagrammatic technique involves the summation of many Feynman diagrams. It has the advantage of analyzing the underlying physics, but is inconvenient numerically, especially in evaluating dynamics and general response functions.

One of the emerging many-particle approaches to quantum transport is the hierarchical equations of motion (HEOM) formalism.[37–41] This approach was constructed originally as a nonperturbative quantum dissipation theory.[42–50] It has been extended recently to coherent quantum-transport problems in which many-fermion systems are in contact with electron reservoir (electrode) environments under arbitrary applied voltage that can be time dependent.[37] The resulting HEOM-based quantum-transport formalism is related naturally to the sequential, cotunneling, and higher-order cotunneling processes.[37,51] As a mathematical equivalence to the Feynman-Vernon influence functional path integral theory,[52,53] HEOM has the advantage in both numerical efficiency and applications to various systems.[38–50] Moreover, the initial system-environment coupling that is not contained in the original path integral formalism can now be accounted for via proper initial conditions to HEOM.

We will show in this paper that inelastic quantum transport can be readily formulated and studied with HEOM. Consider an interacting electronic system embedded in a phonon bath

and sandwiched by two electrodes that serve the source and the drain reservoirs for transport. This situation is covered in the framework of quantum dissipation theory, so it is promising to have the HEOM-based studies of inelastic quantum transport. Nevertheless, the efficiency of HEOM is closely related to the physical issue about system and environment partition of full Hamiltonians. Electron tunneling generally involves the formation of localized polarons, where the tunneling charge is inseparable from the distortion of its accompanying nuclear lattice environment. In this work, we exploit the small polaron transform on the full Hamiltonian for inelastic quantum transport. In Appendix A we present the details of this transformation and the related quantum statistical description of the interacting environments, while in Appendix B we highlight the construction of HEOM for inelastic quantum transport in general. In Sec. II we illustrate the resulting HEOM formalism with the Anderson impurity model of the quantum-transport system, embedded in the Einstein lattice phonon bath. Numerical demonstrations in Sec. III include not only the distinct phonon-assisted features in different tunneling regimes, but also the effect of alternating field versus that of phonon bath temperature on inelastic quantum transport. Our model calculation results would suggest the use of a proper alternating field, applied on either a bias-voltage or the quantum-dot system, to control the overheating problem in mesoscopic quantum-transport devices. The underlying mechanism seeks to modulate the relative phase of transferring electron wave function. We conclude this work in Sec. IV.

II. THE HEOM APPROACH TO INELASTIC QUANTUM TRANSPORT

A. Model

It is well established that the transient coherent electron transport under arbitrary time-dependent bias voltage can be conveniently and accurately studied with the HEOM formalism.[37–41] In the following, we extend this formalism[37] to inelastic quantum-transport systems via the polaron picture. The small polaron transform and the related statistical mechanics description of the correlated electron reservoirs and the phonon bath influence on polaron transport systems are detailed in Appendix A.

For illustration we adopt the Anderson impurity quantum-dot (QD) electronic system, which is coupled with a phonon bath and also with the source and drain electron reservoirs. The reduced polaron system Hamiltonian reads [cf. Eqs. (A13) and (A14)]

$$H = \sum_s (\varepsilon_{0s} - \lambda)\hat{n}_s + (U_0 - 2\lambda)\hat{n}_\uparrow \hat{n}_\downarrow. \tag{1}$$

Here $\hat{n}_s = \hat{a}_s^\dagger \hat{a}_s \equiv \hat{a}_s^+ \hat{a}_s^-$ is the particle number operator in the QD's electronic level of energy ε_s and spin $s = \uparrow$ or $\downarrow$, with the on-dot Coulomb repulsion energy U and the phonon-bath-induced reorganization energy $\lambda \equiv \lambda_{\rm ph}$ of Eq. (A26) in Appendix A. The total composite Hamiltonian assumes the form $H_{\rm total}(t) = H(t) + H'(t)$, with $H'(t)$ the polaron-transformed system-environment coupling in the stochastic reservoirs-and-bath environment interaction picture being given by Eq. (A15):

$$H'(t) = \sum_{\alpha s} \left[\hat{a}_s^+ \hat{F}_{\alpha s}^-(t) e^{i\phi_{\rm ph}(t)} + e^{-i\phi_{\rm ph}(t)} \hat{F}_{\alpha s}^+(t) \hat{a}_s^-\right]. \tag{2}$$

The influence of environment on the reduced polaron system is characterized by the environment correlation functions $\widetilde{C}_{\alpha s}^{\pm}(t,\tau) = \langle \hat{F}_{\alpha s}^{\pm}(t) \hat{F}_{\alpha s}^{\mp}(\tau)\rangle \langle e^{i\phi_{\rm ph}(t)} e^{-i\phi_{\rm ph}(\tau)}\rangle$, i.e., Eq. (A16) with Eq. (A18):

$$\widetilde{C}_{\alpha s}^{\sigma}(t,\tau) = \exp\left[\sigma i \int_\tau^t dt' \Delta_\alpha(t')\right] C_{\alpha s}^{\sigma;{\rm eq}}(t-\tau) \widetilde{C}_{\rm ph}(t-\tau). \tag{3}$$

It is related to electron transfer to/from ($\sigma = +/-$), the system state s through the α lead. The first component in Eq. (3) arises from the external applied chemical potential or bias voltage $V(t) = \Delta_{\rm L}(t) - \Delta_{\rm R}(t)$ that can be time dependent. The last two components are the steady-state contributions from the specified α reservoir and the phonon bath, respectively, with their own thermodynamic equilibrium states.

Adopted further is the Einstein lattice model to describe the phonon bath (see Appendix A 4). It assumes all phonon bath modes are of same frequency Ω. The resulting phonon bath contribution to Eq. (3) is given by Eq. (A29), i.e.,

$$\widetilde{C}_{\rm ph}(t) = \sum_{m=-\infty}^{\infty} A_m e^{-im\Omega t} \approx \sum_{m=-M_{\rm min}}^{M_{\rm max}} A_m e^{-im\Omega t}, \tag{4}$$

with A_m given by Eq. (A30), satisfying $A_m \geqslant 0$ and $\sum_m A_m = 1$. For numerical purposes, we confine $m \in [-M_{\rm min}, M_{\rm max}]$. The Einstein lattice model is rather reasonable at low temperatures. The Huang-Rhys factor $S \equiv \lambda/\Omega$ serves now as the dimensionless measure of electron-phonon coupling strength.

In Eq. (3), $C_{\alpha s}^{\sigma;{\rm eq}}(t-\tau)$ is the equilibrium reservoir correlation function. It is related to the electrode spectral density function $J_{\alpha s}(\omega)$ via the fermionic grand ensemble's fluctuation-dissipation theorem of Eq. (A23), i.e.,

$$C_{\alpha s}^{\sigma;{\rm eq}}(t) = \frac{1}{\pi}\int_{-\infty}^{\infty} d\omega \frac{e^{\sigma i\omega t} J_{\alpha s}(\omega)}{1 - e^{\sigma\beta_\alpha(\omega - \mu_\alpha^{\rm eq})}}, \tag{5}$$

where $\beta_\alpha = 1/(k_B T_\alpha)$ is the inverse temperature of the α lead. The equilibrium chemical potential can be set to $\mu_\alpha^{\rm eq} = 0$ for all leads in the absence of external voltage applied on them. In this work, the temperatures at two reservoirs are set to be the same, $T_{\rm L} = T_{\rm R} = T_{\rm res}$, while the phonon bath temperature $T_{\rm ph}$ can be either larger or smaller than $T_{\rm res}$. Also set the unit with the Planck constant, Boltzmann constant, and electron charge as $\hbar = k_B = e = 1$.

For simplicity, we chose the Drude model for the electrode reservoir spectral density:

$$J_{\alpha s}(\omega) = \frac{\Gamma W^2/2}{\omega^2 + W^2}. \tag{6}$$

Here the system-electrode coupling strength $\Gamma = \Gamma_{\alpha s}$ and the electrode bandwidth $W = W_{\alpha s}$ are set to be symmetric with respect to the leads $\alpha = {\rm L}$ and R and the spins $s = \uparrow$ and $\downarrow$. To construct the HEOM formalism in the coming section, we expand the correlation function of Eq. (5) also in an

exponential series. For Eq. (6) we have

$$C^{\sigma;\mathrm{eq}}_{\alpha s}(t) \approx \sum_{k=0}^{N} \eta^{\sigma}_{k} e^{-\gamma_k t}, \tag{7}$$

with $\gamma_0 = W$ from the Drude pole of $J_{\alpha s}(\omega)$ and $\gamma_{k>0}$ from the poles of Fermi function involved in Eq. (5). In this work, we exploit the $[N-1/N]$ Padé spectrum decomposition of Fermi function.[54,55]

B. The HEOM formalism

The dynamics quantities in the HEOM formalism of quantum transport are a set of well-defined auxiliary density operators (ADOs).[37] The reduced density operator is set to be the zeroth-tier ADO of the hierarchy, i.e., $\rho(t) \equiv \mathrm{tr}_{\mathrm{env}}\rho_{\mathrm{tot}}(t) \equiv \rho^{(0)}(t)$, and it couples to a set of first-tier ADOs, $\{\rho^{(1)}_j\}$. The index j specifies the distinct memory-frequency components of environment correlation functions as decomposed.[37] That is, $j \equiv \{m\sigma\alpha sk\}$ for the decomposition of Eq. (3) with Eqs. (4) and (7). Denote for later use $\bar{m} = -m$, while $\bar{\sigma}$ is the opposite sign of $\sigma = +$ or $-$.

With the detailed derivations presented in Appendix B, we summarize the final HEOM formalism as follows. We denote an nth-tier ADO as[37,41]

$$\rho^{(n)}_{\mathbf{j}} \equiv \rho^{(n)}_{j_1\ldots j_n}; \qquad \forall\, j_r \in \{j\},\ \ j \equiv \{m\sigma\alpha sk\}. \tag{8}$$

Its associated $(n \pm 1)$th-tier ADOs are $\{\rho^{(n+1)}_{\mathbf{j}j} \equiv \rho^{(n+1)}_{j_1\ldots j_n j}\}$ and $\{\rho^{(n-1)}_{\mathbf{j}_r} \equiv \rho^{(n-1)}_{j_1\ldots j_{r-1}j_{r+1}\ldots j_n}\}$, respectively. We have

$$\dot{\rho}^{(n)}_{\mathbf{j}} = -\big[i\mathcal{L} + \gamma^{(n)}_{\mathbf{j}}(t)\big]\rho^{(n)}_{\mathbf{j}} - i\sum_{r=1}^{n}(-)^{n-r}\,\mathcal{C}_{j_r}\,\rho^{(n-1)}_{\mathbf{j}_r} - i\sum_{j;\sigma,s\in j}{}' \mathcal{A}^{\bar{\sigma}}_{s}\,\rho^{(n+1)}_{\mathbf{j}j}, \tag{9}$$

with $\gamma^{(0)} = \rho^{(-1)} = 0$ for the zero-tier ADO or the reduced density operator $\rho = \rho^{(0)}$. The last sum runs only over those $j \neq j_r; r = 1, \ldots, n$. In Eq. (9), $\gamma^{(n)}_{\mathbf{j}}(t)$ collects all the exponents involved,

$$\gamma^{(n)}_{\mathbf{j}}(t) = \sum_{r=1}^{n}[\gamma_k + im\Omega - \sigma i\Delta_{\alpha}(t)]_{m,\sigma,\alpha,s,k\in j_r}, \tag{10}$$

where $\mathcal{A}^{\sigma}_{s}$ and $\mathcal{C}_j$ are the fermionic superoperators, defined via their actions on a fermionic/bosonic operator $\hat{O}$ as

$$\mathcal{A}^{\sigma}_{s}\hat{O} = \big[\hat{a}^{\sigma}_{s}, \hat{O}\big]_{\mp}, \tag{11}$$

$$\mathcal{C}_j\hat{O} = \big(A_m\eta^{\sigma}_{k}\big)\,\hat{a}^{\sigma}_{s}\hat{O} \pm \big(A_{\bar{m}}\eta^{\bar{\sigma}}_{k}\big)^{*}\hat{O}\hat{a}^{\sigma}_{vs}. \tag{12}$$

In particular, $\rho^{(n-1)}_{\mathbf{j}_r}$ and $\rho^{(n+1)}_{\mathbf{j}j}$ in Eq. (9) are both fermionic or bosonic when n is even or odd, respectively.

We conclude the above HEOM formalism with the following remarks:[37]

(i) Fermionic ADO labeling: All involved indices in $\rho^{(n)}_{j_1\ldots j_n}$ should be distinct, and each permutation of them leads to a sign change such that $\rho_{j_2 j_1} = -\rho_{j_1 j_2}$. This also accounts for the sign $(-)^{n-r}$ inside the second sum in Eq. (9). For numerical code, an *ordered* set of indices is to be adopted, together with considering the Hermite conjugated relation below.

(ii) Hermite conjugation (denoting $\bar{j} \equiv \{\bar{m}\bar{\sigma}\alpha sk\}$):

$$\big[\rho^{(n)}_{j_1\ldots j_n}\big]^{\dagger} = \rho^{(n)}_{\bar{j}_n\ldots\bar{j}_1} = (-)^{[\frac{n}{2}]}\rho^{(n)}_{\bar{j}_1\ldots\bar{j}_n}, \tag{13}$$

with $[\frac{n}{2}] \equiv \mathrm{Int}(n/2)$ being the number of index-swapping operations involved.

(iii) Steady-state solutions versus initial values to HEOM: For the cases of time-independent voltage $V = \Delta_{\mathrm{R}} - \Delta_{\mathrm{L}}$ applied on the leads, we search for the nonequilibrium steady-state ADOs with Eq. (9) by setting $\dot{\rho}^{(n)} = 0$ together with the constraint of $\mathrm{tr}\rho^{(0)} = 1$. On the other hand, if the applied bias voltage is also time dependent, on the top of the constant potentials $\Delta_{\alpha}(t) = \Delta_{\alpha} + \delta\Delta(t)$, the steady-state solutions to the HEOM with the constant Δ_{α} will serve as the initial conditions for the subsequent transient properties of ADOs, in response further to the time-dependent $\delta\Delta(t)$.

(iv) The spin-resolved terminal current to central QD system is related to the first-tier ADOs via $\rho^{\sigma}_{\alpha s} \equiv \sum_{m,k}\rho^{(1)}_{j}|_{j=\{m\sigma\alpha sk\}}$ as

$$I_{\alpha s}(t) = -2e\,\mathrm{Im}\big\{\mathrm{tr}\big[\hat{a}_s\,\rho^{+}_{\alpha s}(t)\big]\big\}. \tag{14}$$

Here e denotes the electron charge and the trace is performed for all system degrees of freedom. Note the zero-phonon ($m = 0$) contribution would not be purely elastic and it alone does not satisfy the steady-state current balance relation of $I^{\mathrm{st}}_{\mathrm{L}\,s}(m = 0) = -I^{\mathrm{st}}_{\mathrm{R}\,s}(m = 0)$.

(v) Our recent analysis (to be published) relates further the nth-tier ADOs to the nth moment of transport current. The HEOM construction contains rich information beyond the averaged current and electron occupation number.

(vi) As a consequence of the fermionic ADO labeling as described in (i) above, the highest possible level $L_{\max}$ of tiers amounts to the number K of first-tier ADOs, $\{\rho^{(1)}_j\}$. As $j \equiv \{m\sigma\alpha sk\}$, with $m \in [-M_{\min}, M_{\max}]$ [Eq. (4)] and $k \in [0, N]$ [Eq. (7)], while each σ, α, and s has two choices, we have $K = 2^3(M_{\max} + M_{\min} + 1)(N + 1)$. Apparently, the value of K depends on the accuracy requirement set for the exponential expansions of environment correlation functions in Eqs. (4) and (7).

(vii) In practice, HEOM has to be evaluated with a converged or truncated tier level L. The total number of ADOs is then $\sum_{n=0}^{L}\frac{K!}{n!(K-n)!} \leqslant 2^K$, where the equal sign holds only with the aforementioned highest possible $L_{\max} = K$. Remarkably, HEOM usually converges quantitatively at a low truncation tier level ($L = 2 \sim 3$) for weak to moderately strong system-reservoir coupling strength. The reason is the nonperturbative nature of the HEOM formalism. One important feature of the formalism is that for effective noninteracting systems ($U = 2\lambda$) that are characterized completely by single-particle properties, the resultant HEOM terminates automatically at $L = 2$ without approximation.[37] This feature highlights the fact that the underlying hierarchy construction resolves nonperturbatively the combined effects of e-e interaction, system-reservoir couplings, and non-Markovian memory of reservoir.

(viii) HEOM combined with the small polaron transformation pertains to all the above features, especially those highlighted in (vii). The nonperturbative nature now also supports an accurate and efficient treatment of strong e-ph coupling at the same level of tier truncation. The reason behind this is as

follows. The small polaron transformation absorbs the e-ph coupling of arbitrary strength into effective system-reservoir coupling as Eq. (3), with the phonon factor $\widetilde{C}_{\rm ph}(t)$ [Eq. (A21) for general cases] being $\widetilde{C}_{\rm ph}(t=0)=1$. In other words, the e-ph coupling does not alter the overall strength of system-reservoir coupling but redistributes tunneling electrons with renormalized rates into various inelastic channels associated with phonon emission ($m>0$) and/or absorption ($m<0$) processes, along with the modified zero-phonon ($m=0$) contribution. This is a correct feature of the present HEOM approach, in which the effects of strong e-ph coupling on inelastic quantum transport are treated in a renormalized and also nonperturbative manner via the hierarchy construction as discussed in (vii).

III. NUMERICAL DEMONSTRATIONS

A. General remarks

We will demonstrate the inelastic transport characteristics in terms of differential conductance $dI/dV \sim V$ for some representative Anderson impurity QD systems of Sec. II A. The reduced polaron system, Eq. (1) with $\lambda = S\Omega$, is specified with the renormalized single-particle energy $\varepsilon_s = \varepsilon_{0s} - \lambda$, where $s = \uparrow, \downarrow$ and the effective two-particle coupling $U = U_0 - 2\lambda$ which can be either repulsive or attractive. The electronic system space for numerical evaluation consists of four Fock states $\{|0\rangle, |\uparrow\rangle, |\downarrow\rangle, |\uparrow\downarrow\rangle\}$ with the energies $\{0, \varepsilon_\uparrow, \varepsilon_\downarrow, \varepsilon_{\uparrow\downarrow}\}$, where $\varepsilon_{\uparrow\downarrow} = \varepsilon_\uparrow + \varepsilon_\downarrow + U$. The Fermi energy is set to be $E_f = 0$.

The inelastic transport features of this system can be largely understood based on the polaron energetics of the QD system. The four electronic Fock states are actually four vibronic manifolds, the unoccupied $|0, n_0\rangle$, the single-occupied $|\uparrow, n_s\rangle$ and $|\downarrow, n'_s\rangle$, and the double-occupied $|\uparrow\downarrow, n_d\rangle$, with $n_0, n_s, n'_s, n_d \geqslant 0$ for the phonon states. For a sequential process that adds (removes) one electron to (from) the system, tunneling resonances occur at $\Delta_{\rm L}(-\Delta_{\rm R}) = \varepsilon_s + m\Omega$ and $\varepsilon_s + U + m\Omega$, with $m = \delta n_s$ or $\delta n'_s$ and $m = \delta n_d$, respectively, where $m \geqslant 0$ describes the associated m-phonon emission. Interestingly, phonon absorption ($m < 0$) associated with sequential tunneling would also occur when the phonon bath temperature $T_{\rm ph}$ is higher than the electron reservoir temperature $T_{\rm res}$. In other words, the cold carrier electron transiting from one electrode to another through the QD system can receive energy from the hot phonon thermal bath to assist transport. Moreover, we also anticipate cotunneling resonances to occur at $eV \equiv \Delta_{\rm L} - \Delta_{\rm R} = \varepsilon_{s,m+m'} - \varepsilon_{s,m} = m'\Omega$, i.e., the Stokes Raman transition ($m' > 0$) between two vibronic manifolds, for a positive bias voltage. We will illustrate the above inelastic features in Sec. III B with the HEOM evaluations of differential conductance in the steady-state configuration. In Sec. III C we evaluate the photon-phonon-assisted tunneling characteristics for the cases driven by a terahertz radiation.

We focus on the regime of $\Gamma < \lambda$, in which the system-electrode coupling is relatively weak and the tunneling charge is inseparable from the distortion of nuclear environment. This is often the case with molecule-electron conjunctions. The tunneling charge-induced phonon emission will result in a series of Franck-Condon phonon sidebands in the dI/dV characteristics. To resolve this feature the temperature of the reservoir ($T_{\rm res} = T_{\rm L} = T_{\rm R}$) needs to be low compared with the phonon energy, i.e., $T_{\rm res} < \Omega$. Besides the phonon emission, the tunneling charge may also stimulate phonon absorption when the phonon bath temperature $T_{\rm ph}$ is higher than $T_{\rm res}$. In relation to the zero-phonon peak in dI/dV, the emission and absorption sidebands appear at the high- and low-bias-voltage sides, respectively. The HEOM formalism in Sec. II B is carried out at the tier-2 truncation level. It includes the cotunneling processes and is also numerically accurate for the coupling reservoir parameters considered in the following demonstrations.[37,41] We further have the HEOM formalism explicitly with $|m| \leqslant 2$. Therefore, the sequential tunneling treats only up to two phonon effects, but the cotunneling level treatment can support up to four phonon processes. The above arguments will serve as a basis for the later analysis of phonon bands in the evaluated dI/dV curves.

In this work, we keep the temperature above the Kondo temperature; thus the possible phonon effect on Kondo resonance is not evaluated. Recall the two advanced features highlighted in (vii) and (viii) to the end of Sec. II B. The former or (vii) concerns the nonperturbative nature of the HEOM treatment of system-electrode coupling (and also e-e coupling). The latter or (viii) is about the effect of e-ph coupling, which upon small polaron transformation leads to renormalized tunneling rates to various inelastic channels, without altering the overall effective system-electrode coupling strength. The above two features validate the present HEOM approach and are an accurate evaluation of the strong e-ph coupling effect. For demonstrations, we set the Huang-Rhys parameter $S = 1$ and the phonon energy $\Omega = 1$meV (or internal unit). We chose $\Gamma = 0.05$ meV, with $W = 30$ or 15 meV, to represent the inelastic transport in the wide-band ($W \gg \Gamma$) regime. The bias is applied symmetrically on electrodes, i.e., $\Delta_{\rm L} = -\Delta_{\rm R} = V/2$. The effective single-particle energy assumes degenerate $\varepsilon_\uparrow = \varepsilon_\downarrow = \varepsilon_s$, whose value can be easily tuned in experiments by gate voltage. We chose some representing values of ε_s and temperatures, $T_{\rm res}$ and $T_{\rm ph}$, to demonstrate the inelastic transport characteristics in different regimes.

B. Phonon-assisted tunneling

1. *Sequential tunneling associated with phonon emissions*

Consider the resonant transport where $\Delta_{\rm L} > \varepsilon_s > \Delta_{\rm R}$ and sequential tunneling is dominant when $T_{\rm res} > \Gamma$. For the illustrations in Fig. 1, we set $\varepsilon_s = 0$, $U = 3\ \Omega$, and $\Gamma = 0.05\ \Omega$ at three values of $T = T_{\rm ph} = T_{\rm res}$: (a) 0.25 Ω, (b) 0.1 Ω, and (c) 0.05 Ω, respectively. Apparently, the two zero-phonon bands are peaked at the polaron and the bipolaron resonances, $\Delta_{\rm L} = \varepsilon_s = 0$ and $\Delta_{\rm L} = \varepsilon_s + U = 3\ \Omega$, respectively. The observed m-phonon sidebands to the blue side of the zero-phonon features clearly indicate the stimulated phonon emission ($m > 0$) processes associated with the electron transport. Note that in the spin-nondegenerate case there are four zero-phonon bands centered at $\varepsilon_\uparrow$ ($\varepsilon_\downarrow$) and $\varepsilon_\uparrow + U$ ($\varepsilon_\downarrow + U$) in relation to the spin-up (spin-down) electron tunneling, from the L electrode to the R electrode through the electronic resonance QD levels. The adopted spin-degenerate case in this study highlights the essence of the phonon-assisted features. We have also limited

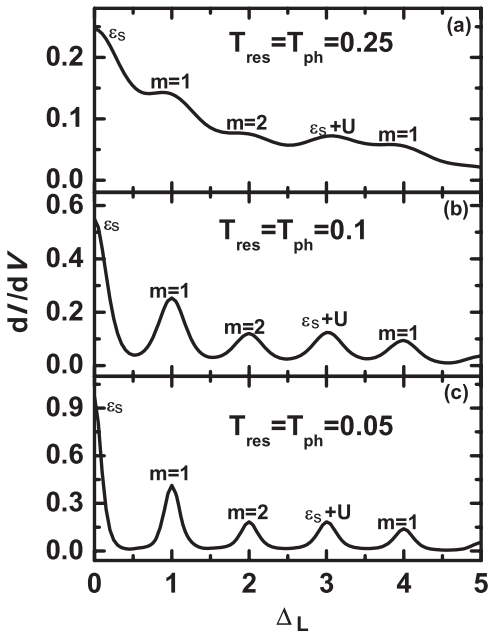

FIG. 1. The differential conductance dI/dV (in units of $\frac{2e^2\Gamma_L\Gamma_R}{\Omega(\Gamma_L+\Gamma_R)}$), as a function of $\Delta_L = eV/2$ (in units of $\Omega = 1$ meV) for the phonon-coupled Anderson impurity QD system, with $\varepsilon_s = 0$, $U = 3\,\Omega$, and $S = 1$, at three values of $T = T_{res} = T_{ph}$: (a) 0.25 Ω, (b) 0.1 Ω, and (c) 0.05 Ω, respectively. Other parameters are $\Gamma = \Gamma_L = \Gamma_R = 0.05\,\Omega$ and $W = 30\,\Omega$.

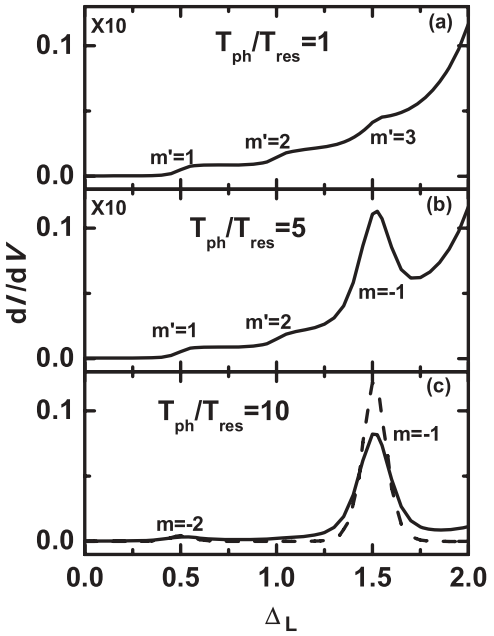

FIG. 2. The same as Fig. 1, but with $\varepsilon_s = 2.5\,\Omega$ and $T_{res} = 0.04\,\Omega$, at three values of T_{ph}/T_{res}: (a) 1, (b) 5, and (c) 10, respectively. The dashed curve in panel (c) is the result of sequential level calculation. Individual resonance is specified with its physical original, being of the Stokes-Raman ($m' > 0$) or phonon-absorption ($m < 0$) assisted tunneling.

the HEOM evaluations with two-phonon ($|m| \leqslant 2$) truncation so that the phonon bands in Fig. 1 are assigned unambiguously.

Evidently, the temperature is a key factor for the appearance of Franck-Condon sidebands. In fact, all phonon-emission peaks would disappear when $T \gtrsim 0.3\,\Omega$ for the QD system of study here. The lower the temperature, the sharper the phonon-emission sidebands will be, with a limiting width of about Γ at $T = 0$. The relative intensity between two-phonon and one-phonon sidebands that are centered at $\varepsilon_s + 2\Omega$ and $\varepsilon_s + \Omega$ is about A_2/A_1, where A_m is given by Eq. (A30). This observation can be used in determining the e-ph coupling strength whenever the Einstein phonon lattice model is valid. Within the limit of zero temperature and wide-band approximation without considering e-ph coupling, the differential conductance at zero bias is $\frac{e^2}{\pi}\frac{4\Gamma_L\Gamma_R}{(\Gamma_L+\Gamma_R)^2}$. The zero-phonon peak of dI/dV can approach this value with the decrease of T.

Note that all results reported in Fig. 1 are based on HEOM at the tier-2 truncation level. Compared to those obtained at the tier-1 level that accounts only for sequential processes, the cotunneling contributions from the tier-2 level calculations are of only quantitative but not qualitative modification. The basic feature of multiple-phonon emissions is contained already in the sequential tunneling description, as it is valid for the resonance transport considered in Fig. 1, where $\Delta_R < \varepsilon_s < \Delta_L$.

2. *Cotunneling with phonon emissions versus sequential tunneling with phonon absorptions*

Consider now the nonresonance ($\varepsilon_s > \Delta_L$) transport regime, where the electronic energy levels of the QD system lie above the bias window. This scenario is readily achievable by applying a gate voltage, for example, to the same QD system considered earlier. We will see the *distinct* features between the cotunneling (resonating at $eV = 2\Delta_L = m'\Omega$) and the photon-absorption-assisted sequential tunneling. The former is of a steplike feature while the latter shows peak(s). For the demonstrations presented in Fig. 2, we set $\varepsilon_s = 2.5\,\Omega$ and $T_{res} = 0.04\,\Omega$, but there are three specified values of T_{ph}/T_{res}. Other parameters remain the same as Fig. 1.

In Fig. 2(a), $T_{ph}/T_{res} = 1$, the same situation as in Fig. 1 but for the nonresonance case. It is observed that differential conductance has a resonance rise at each of $\Delta_L/\Omega = 0.5$, 1, and 1.5, followed by a flat step or smooth rise in between or after. The first two resonance rises, with the centers corresponding to $eV = 2\Delta_L = \Omega$ and $2\,\Omega$, respectively, are unambiguously due to the *cotunneling resonance* mechanism, as detailed in Sec. III A. However, the mechanism underlying the third resonant rise centered at $\Delta_L = 1.5\,\Omega$, is less straightforward. It can be attributed to either the three-phonon-emission ($m' = 3$) assisted cotunneling with $eV = 2\Delta_L = 3\,\Omega$ or the one-phonon-absorption assisted sequential tunneling with $\Delta_L = \varepsilon_s - \Omega = 1.5\,\Omega$; see the related comments in Sec. III A. Note that the present HEOM evaluation takes into account up to two- and four-phonon events in sequential tunneling and cotunneling processes, respectively. To identify the underlying mechanism, we perform the tier-1 truncation HEOM calculation and exclude the one-phonon-absorption assisted sequential tunneling for the observed third resonant rise in Fig. 2(a). Note also that sequential tunneling resonance is characterized by a peak in conductance, while cotunneling resonance is by a steplike feature, as evident from the individual panels of Figs. 1 and 2(a), respectively. These

characteristics are physically related to the resonant versus nonresonant transport regions.

In Figs. 2(b) and 2(c), we set $T_{\rm ph}/T_{\rm res} = 5$ and 10, respectively, while $T_{\rm res} = 0.04\ \Omega$ remains unchanged to mimic the local heating accompanying the current flow through the dot system. The local heating can in turn enhance the probability of phonon-absorption processes, as evident in the observed dI/dV characteristics. For Fig. 2(b), while the first two steplike resonances remain cotunneling in nature, occurring at $eV = 2\Delta_{\rm L} = \Omega$ and $2\ \Omega$, respectively, the third resonance shows a peak feature and arises therefore mainly from sequential tunneling, with the phonon-absorption resonance at $\Delta_{\rm L} = \varepsilon_s - \Omega$. With $T_{\rm ph}$ being enhanced further in Fig. 2(c), the phonon-absorption-assisted sequential processes dominate, resulting in the effective suppression of the cotunneling characteristics. Included in Fig. 2(c) is also the result (dash-curve) of the sequential-tier or tier-1 truncation level of HEOM evaluation to confirm the above analysis.

We have thus detailed the basic $dI/dV \sim V$ features of phonon-assisted tunneling in terms of emission versus absorption and sequential tunneling versus cotunneling characteristics. Reported in Figs. 1 and 2 are the cases with $U > 0$. We have also studied the cases with attractive effective interaction ($U < 0$) and find similar resonance characteristics that are covered at least physically in Figs. 1 and 2.

C. Photon-phonon-assisted tunneling and a possible method of cooling

Transient quantum-transport features under various time-dependent external fields carry much more information than their stationary counterpart. The unified HEOM evaluation of transient current responses had been extensively carried out in the coherent or elastic transport limit.[37–41,56–58] The extension to the inelastic cases is straightforward. In the following, instead of the transient features of current response, we would rather evaluate the cyclically averaged steady-state current response to an oscillatory bias potential applied to the source and drain leads, $\mu_{\rm L}(t) = \Delta_{\rm L} + \Delta\sin(\omega t) = -\mu_{\rm R}(t)$. While this setup can be directly realized in experiments by applying an irradiation wave to the contacts,[59] the underlying physics of modulating the relative electron phase can also be experimentally studied with the irradiation applied on the dots system.[60] In the model study below we will not just reproduce the additional photon-assisted (ω) phenomenon observed in experiments,[59,60] but also highlight its being a possible local cooling method in quantum-transport devices.

Considered in Fig. 3 is the cyclically averaged conductance $d\bar{I}/dV$ (with respect to the time-independent component $V = 2\Delta_{\rm L}/e$), at the long-time Floquet steady-state regime, for the same QD system of Fig. 1, $\varepsilon_s = 0$ and $S = 1$, with $T_{\rm res} = T_{\rm ph} = 0.1\ \Omega$, but setting $U \to \infty$ to avoid the congestion of double-occupancy resonances. The driving frequency is set to be $\omega = 1.65\Omega$, with three specified values of modulation amplitude, $\Delta/\Omega = 1$, 2, and 3. Note that the effective Coulomb coupling U can prolong the system driven by an alternating field to achieve the steady-state limit. For the cases of Fig. 3, the steady-state oscillation is arrived at after about 40 cycles. The photon-phonon-assisted sequential tunneling has the resonances at $\Delta_{\rm L} = \varepsilon_s + n\omega + m\Omega$, as specified by

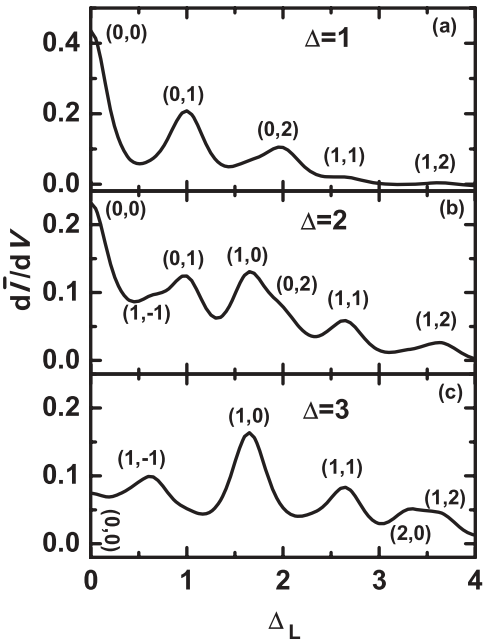

FIG. 3. The cyclically averaged, steady state $d\bar{I}/dV$ as a function of $\Delta_{\rm L} = eV/2$ in response to the alternating-bias-voltage potential $eV + 2\Delta\sin(\omega t)$ applied symmetrically to two leads. Units adopted are the same as Fig. 1. The Anderson impurity QD system has the effective $\varepsilon_s = 0$ and $U \to \infty$, with $S = 1$. The irradiation field carries the frequency $\omega = 1.65\ \Omega$ with the three specified values of amplitude Δ: (a) 1, (b) 2, and (c) 3, respectively. Other parameters are $\Gamma_{\rm L} = \Gamma_{\rm R} = 0.05\ \Omega$, $W = 15\ \Omega$, and $T_{\rm res} = T_{\rm ph} = 0.1\ \Omega$. The label (n,m) specifies the n-photon and m-phonon assisted sequential tunneling process.

(n,m) in Fig. 3, for the n photons associated $|m|$ phonons of emission ($m > 0$) or absorption ($m < 0$) processes in the electron transport. The key features of Fig. 3 are summarized as follows: (i) emergence of the pure photon ($n > 0$ and $m = 0$) and the photon-induced phonon emission ($n,m > 0$) processes in the large-bias-voltage side; (ii) suppression of the zero-photon (or the previous) zero-phonon and m-phonon emission, i.e., the ($n = 0$ and $m \geqslant 0$) processes, operated in the original bias-voltage region; and (iii) emergence of the photon-phonon-absorption assisted tunneling of the ($n > 0, m < 0$) resonance, which would not occur at $T_{\rm res} = T_{\rm ph}$ in the absence of oscillating field (cf. Fig. 1). The above features generally agree with the experimental observations.[59,60] Note that the photon-phonon-assisted tunneling in open QD systems had also been studied using the standard nonequilibrium Green's function approach,[61–63] with the effective interaction U being either neglected or treated in a mean-field approximation. The basic features as discussed above were also reported.[61–63]

The observed features (ii) and (iii) above would also suggest the possibility of applying proper irradiation fields to fight against the potential heating problem associated with quantum transport through mesoscopic systems. Note that the heat capacity of a QD system is usually dominant by phonon lattice bath rather than carrier electrons. Consider now the mesoscopic device operated in the bias-voltage region being of $\Delta_{\rm L} \lesssim \varepsilon_s + 2\Omega$, where heating could occur due to one or two quanta of Ω-phonon energy emitted to the quantum-dot

system. Note the feature (i) discussed previously regarding the emergence of the $(n > 0, m > 0)$ processes causing heating to occur beyond the specified operation region. On the other hand, feature (ii) with regard to the suppression of phonon emission appears right within the operation region. It helps the fight against the QD temperature rise there. Cooling would also happen due to the existence of the photon-phonon-absorption assisted $(n > 0, m < 0)$ processes there, i.e., the feature (iii) of Fig. 3 as discussed earlier. In the absence of oscillating bias potential, the transport electron energy at a given operation bias voltage may fall short of what is needed for efficient transmission. With the additional oscillating bias field, this shortage can now be supplied for by absorbing phonons that result in cooling. The feature (iii) regarding the photon-phonon-absorption assisted tunneling activates this cooling mechanism. Cooling could be achieved via different means and mechanisms.[11] The alternating-bias-assisted cooling as suggested here, or more generally, the control of the relative phase of the transferring electronic wave function, is one of the viable methods and worthy of further exploration.

IV. CONCLUDING REMARKS

We have combined the HEOM formalism[37] with small polaron transformation for inelastic quantum-transport systems. With the Einstein lattice model as an illustration, we have identified the distinct phonon-assisted $dI/dV \sim V$ features, *peaks* versus *steps*, in different tunneling regimes. The characteristic peaks in the sequential tunneling regime are associated with the Franck-Condon sidebands for phonon emissions or absorptions, while the characteristic steps in the cotunneling regime are associated with Raman resonances. We have also studied the effect of external irradiation field versus that of phonon bath temperature on inelastic quantum transport. Our results suggest that applying a suitable alternating bias voltage could be a practical means to fight against the heating problem in mesoscopic quantum-transport devices. Physically, this is to control the relative phase of the transferring electronic wave function, which can also be implemented by applying irradiation fields on quantum wire/dot systems.

HEOM is a versatile and nonperturbative theoretical tool in the study of time-dependent and strongly correlated systems, including inelastic quantum transport, with a broad range of couplings beyond the Einstein lattice model. Interesting problems such as the Kondo physics in quantum impurity systems in the presence of arbitrary phonon lattice environments can be readily studied with the HEOM approach. Note that strong e-ph interaction can also result in a net attraction between electrons and consequently, the Cooper pair generation in superconductor. An HEOM-based, time-dependent density functional theory[37,57] to extend the first-principles calculations to inelastic transport is also in progress.

ACKNOWLEDGMENTS

Support from the University Grants Committee of Hong Kong SAR (No. AoE/P-04/08-2), the NSF of China (No. 21033008), and the National Basic Research Program of China (No. 2011CB921400) is gratefully acknowledged.

APPENDIX A: THE ONSET OF SMALL POLARON TRANSFORM

1. An inelastic quantum-transport model

Consider a molecular wire or quantum-dot system, specified with an arbitrary electronic Hamiltonian H_e, in contact with both electrodes and a phonon bath. The total composite Hamiltonian is then

$$H_T = H_e + H_{res} + H_{e\text{-}res} + H_{ph} + H_{e\text{-}ph}. \tag{A1}$$

In general, the many-electron system Hamiltonian H_e is expressed in terms of the creation ($\hat{a}^\dagger_{\mu s}$) and annihilation ($\hat{a}_{\mu s}$) operators, for an electron in the specified system orbital μ with spin s.

The electrodes serve as electron reservoirs, assuming the Hamiltonian of

$$H_{res} = \sum_\alpha h_\alpha = \sum_{\alpha k s} \epsilon_{\alpha k s} \hat{c}^\dagger_{\alpha k s} \hat{c}_{\alpha k s}. \tag{A2}$$

Here $\hat{c}^\dagger_{\alpha k s}$ ($\hat{c}_{\alpha k s}$) denotes the creation (annihilation) operator for the kth single-electron state with energy $\epsilon_{\alpha k s}$ and spin s in the α electrode. The system reservoir's coupling assumes the transfer type

$$\begin{aligned} H_{e\text{-}res} &= \sum_{\alpha k \mu s} (t^*_{\alpha \mu k s} \hat{a}^\dagger_{\mu s} \hat{c}_{\alpha k s} + t_{\alpha \mu k s} \hat{c}^\dagger_{\alpha k s} \hat{a}_{\mu s}) \\ &\equiv \sum_{\alpha \mu s} (\hat{a}^\dagger_{\mu s} \hat{F}_{\alpha \mu s} + \hat{F}^\dagger_{\alpha \mu s} \hat{a}_{\mu s}), \end{aligned} \tag{A3}$$

with $\hat{F}_{\alpha \mu s} \equiv \sum_k t^*_{\alpha \mu k s} \hat{c}_{\alpha k s}$.

The phonon bath is modeled by a collection of harmonic oscillators:

$$H_{ph} = \frac{1}{2} \sum_j \omega_j (\hat{p}^2_j + \hat{x}^2_j). \tag{A4}$$

The system-phonon bath coupling assumes the form of

$$H_{e\text{-}ph} = -\hat{Q}_e \sum_j c_j \hat{x}_j \equiv -\hat{Q}_e \hat{F}_{ph}. \tag{A5}$$

The electronic system operator $\hat{Q}_e$ here defines the dissipative mode through which the phonon bath acts on the system. In this work, we chose it as the total number operator of the system:

$$\hat{Q}_e = \hat{N}_e \equiv \sum_{\mu s} \hat{n}_{\mu s}. \tag{A6}$$

Note that in the absence of electrode contact, the total number of electrons in the system is conserved. This implies that $[\hat{N}_e, H_e] = 0$. Thus, the dissipative mode specified in Eq. (A6) would not cause energy relaxation if there were no exchange of particles between system and environment. Note also that the statistical nature of the couplings with the electron reservoirs and phonon bath will be characterized later in terms of spectral density functions in Appendix A 3.

2. Small polaron transform and related environment correlation functions

The polaron transform is unitary, with the intention to optimally reduce the effective e-ph coupling in the transformed

$(H_e + H_{ph} + H_{e\text{-}ph})$. This goal is perfectly achievable for a nondemolishing dissipative mode, i.e., $[\hat{Q}_e, H_e] = 0$, as exemplified with $\hat{Q}_e = \hat{N}_e$ [Eq. (A6)], with the celebrated Holstein small polaron transform:

$$\widetilde{O} \equiv e^{i\hat{N}_e\hat{\phi}_{ph}} O e^{-i\hat{N}_e\hat{\phi}_{ph}}, \tag{A7}$$

where

$$\hat{\phi}_{ph} = \sum_j \frac{c_j}{\omega_j}\hat{p}_j. \tag{A8}$$

It satisfies $\dot{\hat{\phi}}_{ph} = -\hat{F}_{ph}$ and $i[\hat{\phi}_{ph}, \hat{F}_{ph}] = \sum_j c_j^2/\omega_j = 2\lambda_{ph}$. The coupling strength adopted here, in terms of phonon-bath-induced reorganization energy λ_{ph}, agrees with its general expression via spectral density [see Eq. (A26)].

The details of the small polaron transform on the total composition Hamiltonian is as follows. Besides $[\hat{N}_e\hat{\phi}_{ph}, H_e] = 0$ and $[\hat{N}_e\hat{\phi}_{ph}, H_{res}] = 0$, Eqs. (A4)–(A6) and (A8) lead to also

$$\begin{aligned} i[\hat{N}_e\hat{\phi}_{ph}, H_{ph}] &= -H_{e\text{-}ph}, \\ i[\hat{N}_e\hat{\phi}_{ph}, H_{e\text{-}ph}] &= -2\lambda_{ph}\hat{N}_e^2, \\ \left[\hat{N}_e\hat{\phi}_{ph}, \hat{N}_e^2\right] &= 0. \end{aligned} \tag{A9}$$

Therefore $\widetilde{H}_e = H_e$, $\widetilde{H}_{res} = H_{res}$,

$$\widetilde{H}_{ph} = H_{ph} - H_{e\text{-}ph} + \lambda_{ph}\hat{N}_e^2, \tag{A10}$$

and

$$\widetilde{H}_{e\text{-}ph} = H_{e\text{-}ph} - 2\lambda_{ph}\hat{N}_e^2. \tag{A11}$$

Using the identities $[\hat{N}_e, \hat{a}_{\mu s}^\dagger] = \hat{a}_{\mu s}^\dagger$ and $[\hat{N}_e, \hat{a}_{\mu s}] = -\hat{a}_{\mu s}$, we obtain further

$$\widetilde{H}_{e\text{-}res} = \sum_{\alpha\mu s}\left(\hat{a}_{\mu s}^\dagger \hat{F}_{\alpha\mu s} e^{i\hat{\phi}_{ph}} + \hat{F}_{\alpha\mu s}^\dagger \hat{a}_{\mu s} e^{-i\hat{\phi}_{ph}}\right). \tag{A12}$$

The small polaron-transformed total composite Hamiltonian is then $\widetilde{H}_T = (H_e - \lambda_{ph}\hat{N}_e^2) + H_{res} + H_{ph} + \widetilde{H}_{e\text{-}res}$. From $\hat{N}_e = \sum_{\mu s}\hat{a}_{\mu s}^\dagger\hat{a}_{\mu s} \equiv \sum_{\mu s}\hat{n}_{\mu s}$, we have

$$\hat{N}_e^2 = \hat{N}_e + 2\sum_{\mu\nu}\hat{n}_{\mu\uparrow}\hat{n}_{\nu\downarrow} + \sum_{\mu,\nu,s}{}' \hat{a}_{\mu s}^\dagger\hat{a}_{\nu s}^\dagger\hat{a}_{\nu s}\hat{a}_{\mu s}. \tag{A13}$$

The last sum runs only those $\mu \neq \nu$, as $(\hat{a}_{\mu s}^\dagger)^2 = 0$.

In line with a stochastic description, we recast the total composite Hamiltonian $\widetilde{H}_T$ in the $(H_{res} + H_{ph})$-based environment interaction picture,

$$H_T(t) = \left(H_e - \lambda_{ph}\hat{N}_e^2\right) + H_{sys\text{-}env}(t), \tag{A14}$$

with the interaction picture of $\widetilde{H}_{e\text{-}res}$ recast as

$$H_{sys\text{-}env}(t) = \sum_{\alpha\mu s}\left[\hat{a}_{\mu s}^\dagger \hat{F}_{\alpha\mu s}(t) e^{i\hat{\phi}_{ph}(t)} + \text{H.c.}\right]. \tag{A15}$$

Here $\hat{F}_{\alpha\mu s}(t) \equiv e^{iH_{res}t}\hat{F}_{\alpha\mu s}e^{-iH_{res}t} = e^{ih_\alpha t}\hat{F}_{\alpha\mu s}e^{-ih_\alpha t}$ and $\hat{\phi}_{ph}(t) \equiv e^{iH_{ph}t}\hat{\phi}_{ph}e^{-iH_{ph}t}$ are stochastic operators in the electron-reservoir and phonon-bath subspaces, respectively. Their effects on the reduced polaron system are characterized completely by their correlation functions.

For the sake of bookkeeping, we introduce $\sigma = -$ or $+$ and $\bar{\sigma}$ the opposite sign of σ, in relation to the electron tunneling into or out of the central system through leads. Denote also $\hat{F}_{\alpha\mu s}^+ \equiv \hat{F}_{\alpha\mu s}^\dagger \equiv (\hat{F}_{\alpha\mu s}^-)^\dagger$. The environment correlation functions then read

$$\begin{aligned} \widetilde{C}_{\alpha\mu\nu s}^\sigma(t,\tau) &\equiv \left\langle\left[\hat{F}_{\alpha\mu s}^\sigma(t) e^{\bar{\sigma} i\phi_{ph}(t)}\right]\left[\hat{F}_{\alpha\nu s}^{\bar{\sigma}}(\tau) e^{\sigma i\phi_{ph}(\tau)}\right]\right\rangle_{env} \\ &= C_{\alpha\mu\nu s}^\sigma(t,\tau)\widetilde{C}_{ph}(t-\tau). \end{aligned} \tag{A16}$$

It contains both the electron reservoir and the phonon bath components.

The electron reservoir correlation function is

$$C_{\alpha\mu\nu s}^\sigma(t,\tau) = \left\langle \hat{F}_{\alpha\mu s}^\sigma(t)\hat{F}_{\alpha s\nu}^{\bar{\sigma}}(\tau)\right\rangle_\alpha. \tag{A17}$$

Here, $\langle O\rangle_\alpha \equiv \text{tr}_\alpha(O\rho_\alpha^\beta)$ denotes the thermodynamic average over the grand canonical ensemble density operator of $\rho_\alpha^\beta \propto e^{-\beta(h_\alpha - \mu_\alpha\hat{N}_\alpha)}$ for the α reservoir under chemical potential μ_α. Apparently, the number operator $\hat{N}_\alpha$ of the electrons in the α reservoir satisfies $[h_\alpha, \hat{N}_\alpha] = 0$. It is about the electron number conservation in an isolated electrode. In the presence of time-dependent external chemical potential $\Delta_\alpha(t)$ applied to the electrode α, the interaction reservoir correlation in Eq. (A17) is nonstationary. In this work we adopt the adiabatic ansatz that neglects the plasmon effects by which the electrode Hamiltonian assumes $h_\alpha + \Delta_\alpha(t)\hat{N}_\alpha$, with the electrode state energy of $\epsilon_{\alpha k s} + \Delta_\alpha(t)$, while the relative state distribution or ρ_α^β remains unchanged. It results in

$$C_{\alpha\mu\nu s}^\sigma(t,\tau) = \exp\left[\sigma i\int_\tau^t dt'\Delta_\alpha(t')\right] C_{\alpha\mu\nu s}^{\sigma;eq}(t-\tau), \tag{A18}$$

where $C_{\alpha\mu\nu s}^{\sigma;eq}(t-\tau)$ denotes the equilibrium counterpart.

The phonon bath contribution in Eq. (A16) reads

$$\widetilde{C}_{ph}(t-\tau) = \langle e^{\bar{\sigma} i\hat{\phi}_{ph}(t)} e^{\sigma i\hat{\phi}_{ph}(\tau)}\rangle_{ph}. \tag{A19}$$

Here, $\langle O\rangle_{ph} \equiv \text{tr}_B(Oe^{-\beta H_{ph}})/\text{tr}_B e^{-\beta H_{ph}}$ denotes the thermodynamic average over the canonical ensemble of the phonon bath. The Wick's theorem in the Gaussian statistics leads to $\widetilde{C}_{ph}(t-\tau) = \exp[\Phi_{ph}(t-\tau)]$, with $\Phi_{ph}(t) = \langle\hat{\phi}_{ph}(t)\hat{\phi}_{ph}(0)\rangle_{ph} - \langle\hat{\phi}_{ph}^2\rangle_{ph}$. Note that before the polaron transform the electron-phonon coupling is given by Eq. (A5) and the phonon bath correlation function reads

$$C_{ph}(t) \equiv \langle\hat{F}_{ph}(t)\hat{F}_{ph}(0)\rangle_{ph}. \tag{A20}$$

To establish the relation between $\widetilde{C}_{ph}(t)$ and $C_{ph}(t)$, we exploit the identity $\langle\dot{A}(t)B(0)\rangle = -\langle A(t)\dot{B}(0)\rangle$ in the thermodynamic average. Thus, that $\dot{\hat{\phi}}_{ph}(t) = -\hat{F}_{ph}(t)$ leads to $\ddot{\Phi}(t) = -\langle\dot{\hat{\phi}}_{ph}(t)\dot{\hat{\phi}}_{ph}(0)\rangle_{ph} = -C_{ph}(t)$. The initial conditions are $\Phi(0) = 0$ and $\dot{\Phi}(0) = -\langle\hat{F}_{ph}\hat{\phi}_{ph}\rangle_{ph} = -i\lambda_{ph}$. The second identity is obtained by using the facts that $\langle\{\hat{F}_{ph}, \hat{\phi}_{ph}\}\rangle_{ph} = 0$ and $\langle[\hat{F}_{ph}, \hat{\phi}_{ph}]\rangle_{ph} = i2\lambda_{ph}$. We obtain therefore

$$\widetilde{C}_{ph}(t) = \exp\left[-i\lambda_{ph}t - \int_0^t d\tau\int_0^\tau d\tau' C_{ph}(\tau')\right]. \tag{A21}$$

3. Environment spectral density functions and fluctuation-dissipation theorems

In the thermodynamics limit or Gaussian statistics, the environmental influence is completely characterized by the spectral density functions. They will be defined formally through the

anticommutator/commutator of involving fermionic/bosonic stochastic operators.

The spectral density functions for the α-electrode influence are

$$J_{\alpha\mu\nu s}(\omega) \equiv \frac{1}{2}\int_{-\infty}^{\infty} dt\, e^{i\omega t}\langle\{\hat{F}_{\alpha\mu s}(t), \hat{F}^{\dagger}_{\alpha s\nu}(0)\}\rangle_{\alpha}. \quad \text{(A22)}$$

This definition is consistent with the conventional expression of $J_{\alpha\mu\nu s}(\omega) = \pi\sum_k t^*_{\alpha\mu ks}t_{\alpha\nu ks}\delta(\omega-\epsilon_{\alpha ks})$ for the linear coupling of the noninteracting reservoir. The equilibrium part of the reservoir correlation function $C^{\sigma;\mathrm{eq}}_{\alpha\mu s\nu}(t-\tau)$ [Eq. (A18)] is determined via the fermionic grand ensemble's fluctuation-dissipation theorem:

$$C^{\sigma;\mathrm{eq}}_{\alpha\mu\nu s}(t) = \frac{1}{\pi}\int_{-\infty}^{\infty} d\omega \frac{e^{\sigma i\omega t}J^{\sigma}_{\alpha\mu\nu s}(\omega)}{1-e^{\sigma\beta(\omega-\mu^{\mathrm{eq}}_{\alpha})}}, \quad \text{(A23)}$$

where $J^{-}_{\alpha\mu\nu s}(\omega) = J^{+}_{\alpha\nu\mu s}(\omega) = J_{\alpha\mu\nu s}(\omega)$.

The spectral density for the phonon bath interaction in Eq. (A5) before polaron transformation is

$$J_{\mathrm{ph}}(\omega) \equiv \frac{1}{2}\int_{-\infty}^{\infty} dt\, e^{i\omega t}\langle[\hat{F}_{\mathrm{ph}}(t), \hat{F}_{\mathrm{ph}}(0)]\rangle_{\mathrm{ph}}. \quad \text{(A24)}$$

It assumes $J_{\mathrm{ph}}(\omega) = \frac{1}{2}\pi\sum_j |c_j|^2[\delta(\omega-\omega_j)-\delta(\omega+\omega_j)]$ for the linear coupling of a harmonic phonon bath. The interacting phonon bath correlation function $C_{\mathrm{ph}}(t)$ is then determined via the bosonic canonical ensemble's fluctuation-dissipation theorem:

$$C_{\mathrm{ph}}(t) = \frac{1}{\pi}\int_{-\infty}^{\infty} d\omega \frac{e^{-i\omega t}J_{\mathrm{ph}}(\omega)}{1-e^{-\beta\omega}}. \quad \text{(A25)}$$

It is also easy to verify that the phonon-bath-induced reorganization energy λ_{ph} specified earlier follows the more general definition of

$$\lambda_{\mathrm{ph}} \equiv \frac{1}{2\pi}\int_{-\infty}^{\infty} d\omega \frac{J_{\mathrm{ph}}(\omega)}{\omega}. \quad \text{(A26)}$$

We have thus completed the small polaron transform of a transport system in which the reduced polaron system Hamiltonian is given by $H_{\mathrm{e}} - \lambda_{\mathrm{ph}}\hat{N}^2_{\mathrm{e}}$. The effects of interacting environment on the reduced system are dictated by the correlation functions in Eq. (A16), $\widetilde{C}^{\sigma}_{\alpha\mu\nu s}(t,\tau) = C^{\sigma}_{\alpha\mu\nu s}(t,\tau)\widetilde{C}_{\mathrm{ph}}(t-\tau)$, with the two components being specified by Eq. (A18) and Eq. (A21), respectively. The involved equilibrium correlation functions before polaron transformation are further related to the spectral density functions $J_{\alpha\mu\nu s}(\omega)$ [Eq. (A22)] and $J_{\mathrm{ph}}(\omega)$ [Eq. (A24)] via the corresponding fluctuation-dissipation theorem expressions.

4. The Einstein phonon bath model

To illustrate the polaron transform theory presented in the previous subsections of this Appendix, let us consider the phonon bath spectral density the form of

$$J_{\mathrm{ph}}(\omega) = \pi\lambda_{\mathrm{ph}}\omega[\delta(\omega-\Omega)+\delta(\omega+\Omega)]. \quad \text{(A27)}$$

This is the Einstein lattice model, assuming all phonon frequencies are the same $\{\omega_j = \Omega\}$. The coupling strength parameter in Eq. (A27) follows its definition of Eq. (A26). The Huang-Rhys factor amounts to $\lambda_{\mathrm{ph}}/\Omega \equiv S$.

Substituting Eq. (A27) into Eq. (A25) leads to

$$C_{\mathrm{ph}}(t) = \lambda_{\mathrm{ph}}\Omega[(\bar{N}+1)e^{-i\Omega t} + \bar{N}e^{i\Omega t}], \quad \text{(A28)}$$

with $\bar{N} = 1/(e^{\beta\Omega}-1)$ being the mean occupation number. It results in

$$\begin{aligned}\int_0^t d\tau\int_0^{\tau} d\tau' C_{\mathrm{ph}}(\tau') &= \frac{\lambda_{\mathrm{ph}}}{\Omega}[(\bar{N}+1)(1-e^{-i\Omega t}-i\Omega t)+\bar{N}(1-e^{i\Omega t}+i\Omega t)]\\ &= -i\lambda_{\mathrm{ph}}t + S[(\bar{N}+1)(1-e^{-i\Omega t})+\bar{N}(1-e^{i\Omega t})].\end{aligned}$$

Therefore Eq. (A21) becomes

$$\begin{aligned}\widetilde{C}_{\mathrm{ph}}(t) &= e^{-S[(\bar{N}+1)(1-e^{-i\Omega t})+\bar{N}(1-e^{i\Omega t})]}\\ &= \sum_{m=-\infty}^{\infty} A_m e^{-im\Omega t},\end{aligned} \quad \text{(A29)}$$

with

$$A_m = \begin{cases}(\bar{N}+1)^m\bar{A}_m & \text{if} \quad m \geqslant 0\\ \bar{N}^{-m}\bar{A}_{-m} & \text{if} \quad m < 0\end{cases}, \quad \text{(A30)}$$

where

$$\bar{A}_{m\geqslant 0} = e^{-S(2\bar{N}+1)}\sum_{k=0}^{\infty}\frac{[S\bar{N}(\bar{N}+1)]^k S^{k+m}}{k!(k+m)!}. \quad \text{(A31)}$$

Apparently, $\sum_m A_m = \tilde{C}_{\mathrm{ph}}(0) = 1$. Note that $I_m(z) = \sum_{k=0}^{\infty}\frac{1}{k!\Gamma(m+k+1)}(z/2)^{m+2k}$; these coefficients can also be expressed in terms of the modified Bessel functions of the first kind $I_m(z)$. In the zero-temperature limit $\bar{N} = 0$, Eq. (A30) with Eq. (A31) reduces to $A_{m<0} = 0$ and $A_{m\geqslant 0} = e^{-S}S^m/m!$, the Poisson distribution.

APPENDIX B: THE HEOM FORMALISM VERSUS PATH INTEGRAL THEORY

1. Influence functional path integral formalism

It is well known that the reduced density operator, $\rho(t) \equiv \mathrm{tr}_{\mathrm{env}}\rho_{\mathrm{T}}(t)$, can be formulated with the Feynman–Vernon influence functional path integral theory[52,53] or its equivalent HEOM formalism.[37,45,46] This formalism is exact, as long as the influence of environment can be completely characterized by the two-time correlation functions, even nonstationary such as Eq. (A16). In contact with the total Hamiltonian of Eq. (A14) and the environment correlation functions of Eq. (A16), we summarize the path integral formalism in this subsection while constructing its equivalent HEOM in Appendix B 2, respectively.

Let $\mathcal{U}(t,t_0)$ be the reduced Liouville-space propagator, by which

$$\rho(t) \equiv \mathcal{U}(t,t_0)\rho(t_0). \quad \text{(B1)}$$

In a path integral formalism of quantum dynamics of open systems, the subspace of the reduced system should be assigned with a specific representation. We denote $\{|\psi\rangle\}$ as a generic basis set, and $\boldsymbol{\psi} \equiv (\psi,\psi')$. Therefore, $\rho(\boldsymbol{\psi},t) \equiv \rho(\psi,\psi',t) \equiv \langle\psi|\rho(t)|\psi'\rangle$. The corresponding reduced Liouville-space propagator in the path integral

formulation can be expressed as[52]

$$\mathcal{U}(\boldsymbol{\psi},t;\boldsymbol{\psi}_0,t_0)=\int_{\boldsymbol{\psi}_0[t_0]}^{\boldsymbol{\psi}[t]}\mathcal{D}\boldsymbol{\psi}\; e^{iS[\psi]}\,\mathcal{F}[\boldsymbol{\psi}]\,e^{-iS[\psi']}. \tag{B2}$$

Here, $S[\psi]$ is the classical action functional of the reduced system, evaluated along a path $\psi(\tau)$, subject to the constraint that the two ending points $\psi(t_0)=\psi_0$ and $\psi(t)=\psi$ are fixed. We denote $\psi(\tau)$ and $\psi'(\tau)$ the forward and backward paths in the integral evolution, for the left ket and right bra sides of ρ, respectively. In the absence of environment, i.e., setting $H_{\text{sys-env}}(t)=0$ in Eq. (A14), $\mathcal{F}[\boldsymbol{\psi}]=1$, with Eq. (B2) being nothing but $\partial_t\mathcal{U}=-i\mathcal{L}U$, or equivalently, the Liouville-von Neumann equation, $\dot\rho(t)=-i\mathcal{L}\rho=-i[H,\rho]$. The reduced system here refers to the polaron so that $H=H_{\rm e}-\lambda_{\rm ph}\hat N_{\rm e}^2$, the first term in Eq. (A14).

The key quantity in Eq. (B2) is the influence functional $\mathcal{F}[\boldsymbol{\psi}]$. It is determined by the system-environment coupling Hamiltonian $H_{\text{sys-env}}(t)$ in Eq. (A14), along with the two-time correlation functions of environment as Eq. (A16). In relation to HEOM, we introduce further the dissipation functional $\mathcal{R}[\tau;\{\boldsymbol{\psi}\}]$ by which $\partial_t\mathcal{F}=-\mathcal{R}F$, or

$$\mathcal{F}[\boldsymbol{\psi}]\equiv\exp\left\{-\int_{t_0}^{t}d\tau\;\mathcal{R}[\tau;\{\boldsymbol{\psi}\}]\right\}. \tag{B3}$$

Through the cumulant expression of the influence functional, we obtain

$$\mathcal{R}[t;\{\boldsymbol{\psi}\}]=i\sum_{\sigma\alpha\mu s}\mathcal{A}^{\bar\sigma}_{\mu s}[\boldsymbol{\psi}(t)]\,\mathcal{B}^{\sigma}_{\alpha\mu s}[t;\{\boldsymbol{\psi}\}], \tag{B4}$$

where $\bar\sigma$ refers to the opposite sign of $\sigma=+$ or $-$:

$$\mathcal{A}^{\sigma}_{\mu s}[\boldsymbol{\psi}(t)]=a^{\sigma}_{\mu s}[\psi(t)]+a^{\sigma}_{\mu s}[\psi'(t)], \tag{B5}$$

$$\mathcal{B}^{\sigma}_{\alpha\mu s}[t;\{\boldsymbol{\psi}\}]=-i\left\{B^{\sigma}_{\alpha\mu s}[t;\{\psi\}]-B'^{\sigma}_{\alpha\mu s}[t;\{\psi'\}]\right\}, \tag{B6}$$

with

$$B^{\sigma}_{\alpha\mu s}[t;\{\psi\}]=\sum_{\nu}\int_{t_0}^{t}d\tau\;\widetilde{C}^{\sigma}_{\alpha s\mu\nu}(t,\tau)\,a^{\sigma}_{\nu s}[\psi(\tau)],$$

$$B'^{\sigma}_{\alpha\mu s}[t;\{\psi'\}]=\sum_{\nu}\int_{t_0}^{t}d\tau\;\left[\widetilde{C}^{\bar\sigma}_{\alpha s\mu\nu}(t,\tau)\right]^{*}a^{\sigma}_{\nu s}[\psi'(\tau)]. \tag{B7}$$

The above equations complete the influence functional path integral theory of reduced system dynamics.

Note that for the fermionic $\{\hat a^{\sigma}_{\mu s}\}$ operators, their path-integral representations $\{a^{\sigma}_{\mu s}[\psi(t)]\}$ are *not* c numbers but Grassmann variables.[53,64] Consequently, the quantities defined in Eqs. (B5)–(B7) are all Grassmann variables, satisfying the algebraic rule of $xy=-yx$. In particular, we have $(\mathcal{B}^{\sigma}_{\alpha\mu s})^2=0$.

Note also that the $\mathcal{A}$ term [Eq. (B5)] depends only on the end points of the path and thus have the explicit operator-level form, while the $\mathcal{B}$ term [Eq. (B6)] of the dissipation functional contains memory and does not support a simple operator-level expression. We may therefore recast $\partial_t\mathcal{F}=-\mathcal{R}F$ as

$$\begin{aligned}\partial_t\mathcal{F}&=-i\sum_{\sigma\alpha\mu s}\mathcal{A}^{\bar\sigma}_{\mu s}[\boldsymbol{\psi}(t)]\,\mathcal{B}^{\sigma}_{\alpha\mu s}[t;\{\boldsymbol{\psi}\}]\mathcal{F}\\&\equiv-i\sum_{\sigma\alpha\mu s}\mathcal{A}^{\bar\sigma}_{\mu s}[\boldsymbol{\psi}(t)]\,\mathcal{F}^{\sigma}_{\alpha\mu s}[t;\{\boldsymbol{\psi}\}],\end{aligned} \tag{B8}$$

with $\mathcal{F}^{\sigma}_{\alpha\mu s}\equiv\mathcal{B}^{\sigma}_{\alpha\mu s}\mathcal{F}$ defining a first-tier auxiliary influence functional. It in turn defines the first-tier auxiliary propagator $\mathcal{U}^{\sigma}_{\alpha\mu s}(\boldsymbol{\psi},t;\boldsymbol{\psi}_0,t_0)$ and then the first-tier auxiliary density operator $\rho^{\sigma}_{\alpha\mu s}(t)$ similarly as Eqs. (B2) and (B1), respectively. Consequently, Eq. (B8) amounts to the following equation of motion:

$$\dot\rho(t)=-i\mathcal{L}\rho(t)-i\sum_{\sigma\alpha\mu s}\mathcal{A}^{\bar\sigma}_{\mu s}\rho^{\sigma}_{\alpha\mu s}(t). \tag{B9}$$

$\mathcal{A}^{\sigma}_{\mu s}$ is now the fermionic superoperator, with the path integral expression of Eq. (B5). As only the terminal path points are involved, it can be equivalently defined via its action on a fermionic/bosonic operator $\hat O$ as

$$\mathcal{A}^{\sigma}_{\mu s}\hat O=\left[a^{\sigma}_{\mu s},\hat O\right]_{\mp}. \tag{B10}$$

In particular, $\mathcal{A}^{\bar\sigma}_{\mu s}\rho^{\sigma}_{\alpha\mu s}(t)=[a^{\sigma}_{\mu s},\rho^{\sigma}_{\alpha\mu s}(t)]$ in Eq. (B9), as the first-tier auxiliary density operator $\rho^{\sigma}_{\alpha\mu s}(t)$ is fermionic.

To continue, we take the time derivative on $\rho^{\sigma}_{\alpha\mu s}(t)$ or equivalently on its influence functional $\mathcal{F}^{\sigma}_{\alpha\mu s}\equiv\mathcal{B}^{\sigma}_{\alpha\mu s}\mathcal{F}$:

$$\begin{aligned}\partial_t\mathcal{F}^{\sigma}_{\alpha\mu s}&=\left(\partial_t\mathcal{B}^{\sigma}_{\alpha\mu s}\right)\mathcal{F}+\mathcal{B}^{\sigma}_{\alpha\mu s}(\partial_t\mathcal{F})\\&=\left(\partial_t\mathcal{B}^{\sigma}_{\alpha\mu s}\right)\mathcal{F}-i\sum_{\sigma'\alpha'\mu's'}\mathcal{A}^{\bar\sigma'}_{\mu's'}\,\mathcal{B}^{\sigma'}_{\alpha'\mu's'}\mathcal{B}^{\sigma}_{\alpha\mu s}\mathcal{F}.\end{aligned} \tag{B11}$$

The second expression is obtained by using the identity of $\partial_t\mathcal{F}=-\mathcal{R}F$ together with Eq. (B4). We may define $\mathcal{F}^{\sigma,\sigma'}_{\alpha\mu s,\alpha'\mu's'}\equiv\mathcal{B}^{\sigma'}_{\alpha'\mu's'}\mathcal{B}^{\sigma}_{\alpha\mu s}\mathcal{F}$ as a second-tier auxiliary influence functional. It implies that the $\partial_t\mathcal{F}$ part always leads to the tier-up dependence.

Consider now the role of $\partial_t\mathcal{B}^{\sigma}_{\alpha\mu s}$ to Eq. (B11). From Eqs. (B6) and (B7) we have

$$\partial_t\mathcal{B}^{\sigma}_{\alpha\mu s}[t;\{\boldsymbol{\psi}\}]=\widetilde{\mathcal{B}}^{\sigma}_{\alpha\mu s}[t;\{\boldsymbol{\psi}\}]-i\mathcal{C}^{\sigma}_{\alpha\mu s}[\boldsymbol{\psi}(t)]. \tag{B12}$$

The $\mathcal{C}$ term depends only on terminal points of the path integral and is given by[37]

$$\mathcal{C}^{\sigma}_{\alpha\mu s}[\boldsymbol{\psi}(t)]=\sum_{\nu}\left\{C^{0,\sigma}_{\alpha\mu\nu s}a^{\sigma}_{\nu s}[\psi(t)]-C^{0,\bar\sigma}_{\alpha\nu\mu s}a^{\sigma}_{\nu s}[\psi'(t)]\right\}, \tag{B13}$$

with $C^{0,\sigma}_{\alpha\mu\nu s}\equiv C^{\sigma,\text{eq}}_{\alpha\mu\nu s}(t=0)=\widetilde{C}^{\sigma}_{\alpha\mu\nu s}(t,t)=[C^{0,\sigma}_{\alpha\nu\mu s}]^*$ being exploited. Like the $\mathcal{A}^{\sigma}_{\alpha\mu s}$ of Eqs. (B5) or (B10), the Grassmann variable $\mathcal{C}^{\sigma}_{\alpha\mu s}[\boldsymbol{\psi}(t)]$ of Eq. (B13) also has a simple operator-level expression. Making contact with Eq. (B11), the $\mathcal{C}$ term from Eq. (B12) leads to the tier-down dependence.

The memory-containing part $\widetilde{\mathcal{B}}^{\sigma}_{\alpha\mu s}$ in Eq. (B12) is defined similarly as Eqs. (B6) and (B7), but with $\widetilde{C}^{\sigma}_{\alpha\mu\nu s}(t,\tau)$ there being replaced with $\partial_t\widetilde{C}^{\sigma}_{\alpha\mu\nu s}(t,\tau)$, resulting in the term $\widetilde{\mathcal{B}}^{\sigma}_{\alpha\mu s}\mathcal{F}$ outside the hierarchy in Eq. (B11). Several methods have been proposed to bring these terms back to the desired hierarchy construction.[37,41] Apparently, the exponential-like expansion of $\widetilde{C}^{\sigma}_{\alpha\mu\nu s}(t,\tau)$ is the most straightforward choice whenever temperature is nonzero.

2. Construction of the HEOM formalism

For illustration, we detail below the HEOM construction for the polaron transport system in Sec. II. As the system considered there consists of only spin levels, the orbital μ and ν indexes are removed hereafter. However, we allow the system-electrode couplings to be spin and lead dependent,

with $J_{\alpha s}(\omega) = \frac{\Gamma_{\alpha s} W_{\alpha s}^2/2}{(\omega-\Omega_{\alpha s})^2+W_{\alpha s}^2}$, rather than Eq. (6), and thus the parameters of $\gamma_{\alpha sk}^{\sigma}$ and $\eta_{\alpha sk}^{\sigma}$ for the exponential expansion of Eq. (7). It is easy to verify that $(\gamma_{\alpha sk}^{\bar\sigma})^* = \gamma_{\alpha sk}^{\sigma}$. We will see soon that the above generalization does not increase the number of equations in the final HEOM formalism.

To proceed, let $\tilde\gamma_{\alpha sk}^{m\sigma} \equiv \gamma_{\alpha sk}^{\sigma} + im\Omega$ and $\tilde\eta_{\alpha sk}^{m\sigma} \equiv A_m \eta_{\alpha sk}^{\sigma}$, by which the environment correlation function $C_{\alpha s}^{\sigma}(t,\tau)$, Eq. (3) with Eqs. (4) and (7), can be recast as

$$\widetilde{C}_{\alpha s}^{\sigma}(t,\tau) = \sum_{m,k} \tilde\eta_{\alpha sk}^{m\sigma}\, e^{\sigma i\int_\tau^t dt'\Delta_\alpha(t')} e^{-\tilde\gamma_{\alpha sk}^{m\sigma}(t-\tau)}. \tag{B14}$$

Note that $(\tilde\gamma_{\alpha sk}^{\bar m\bar\sigma})^* = \tilde\gamma_{\alpha sk}^{m\sigma}$, where $\bar m = -m$ and $\bar\sigma$ the opposite sign of $\sigma = +$ or $-$. We have

$$\big[\widetilde{C}_{\alpha s}^{\bar\sigma}(t,\tau)\big]^* = \sum_{m,k} \big(\tilde\eta_{\alpha sk}^{\bar m\bar\sigma}\big)^* e^{\sigma i\int_\tau^t dt'\Delta_\alpha(t')} e^{-\tilde\gamma_{\alpha sk}^{m\sigma}(t-\tau)}. \tag{B15}$$

For the sake of bookkeeping, we introduce the abbreviation

$$j \equiv \{m\sigma\alpha sk\} \quad\text{and}\quad \bar j \equiv \{\bar m\bar\sigma\alpha sk\},$$

so that $\tilde\gamma_j \equiv \tilde\gamma_{\alpha sk}^{m\sigma}$, $\tilde\eta_j \equiv \tilde\eta_{\alpha sk}^{m\sigma}$ and $(\tilde\eta_{\alpha sk}^{\bar m\bar\sigma})^* = \tilde\eta_{\bar j}^*$. We may recast Eq. (B4) with Eqs. (B5)–(B7) as

$$\mathcal{R}[t;\{\boldsymbol{\psi}\}] = i \sum_{j;\sigma,s\in j} \mathcal{A}_s^{\bar\sigma}[\boldsymbol{\psi}(t)]\, \mathcal{B}_j[t;\{\boldsymbol{\psi}\}], \tag{B16}$$

where $\mathcal{A}_s^{\sigma}[\boldsymbol{\psi}(t)] = a_s^{\sigma}[\psi(t)] + a_s^{\sigma}[\psi'(t)]$ and

$$\mathcal{B}_j[t;\{\boldsymbol{\psi}\}] = -i\{\tilde\eta_j B_j[t;\{\psi\}] - \tilde\eta_{\bar j}^* B_j[t;\{\psi'\}]\}, \tag{B17}$$

with

$$B_j[t;\{\psi\}] = \int_{t_0}^{t} d\tau\, e^{\sigma i\int_\tau^t dt'\Delta_\alpha(t')} e^{-\tilde\gamma_j(t-\tau)} a_s^{\sigma}[\psi(\tau)]. \tag{B18}$$

We have

$$\begin{aligned}\partial_t \mathcal{B}_j[t;\{\boldsymbol{\psi}\}] = &-[\tilde\gamma_j - \sigma i\Delta_\alpha(t)]\mathcal{B}_j[t;\{\boldsymbol{\psi}\}] \\ &- i\mathcal{C}_j[\boldsymbol{\psi}(t)],\end{aligned} \tag{B19}$$

with

$$\mathcal{C}_j[\boldsymbol{\psi}(t)] = \tilde\eta_j a_s^{\sigma}[\psi(t)] - \tilde\eta_{\bar j}^* a_s^{\sigma}[\psi'(t)]. \tag{B20}$$

An nth-tier ADO can be defined generically as

$$\rho_{\mathbf{j}}^{(n)}(t) \equiv \rho_{j_1\ldots j_n}^{(n)} \equiv \mathcal{U}_{\mathbf{j}}^{(n)}(t,t_0)\rho(t_0), \tag{B21}$$

with the path integral expressions of

$$\mathcal{U}_{\mathbf{j}}^{(n)}(\boldsymbol{\psi},t;\boldsymbol{\psi}_0,t_0) = \int_{\boldsymbol{\psi}_0[t_0]}^{\boldsymbol{\psi}[t]} \mathcal{D}\boldsymbol{\psi}\, e^{iS[\psi]} \mathcal{F}_{\mathbf{j}}^{(n)}[\boldsymbol{\psi}] e^{-iS[\psi']} \tag{B22}$$

and

$$\mathcal{F}_{\mathbf{j}}^{(n)} = \mathcal{F}_{j_1 j_2\ldots j_n}^{(n)} = \mathcal{B}_{j_n}\ldots\mathcal{B}_{j_2}\mathcal{B}_{j_1}\mathcal{F}. \tag{B23}$$

As the Grassmann nature of individual $\mathcal{B}_{j_r}$, all involving indices $\{j_r; r = 1,\ldots,n\}$ in $\mathcal{F}_{\mathbf{j}}^{(n)} = \mathcal{F}_{j_1 j_2\ldots j_n}^{(n)}$, should be distinct, and each permutation of indices leads to a sign change; see remarks after Eq. (12).

The HEOM in terms of auxiliary influence functionals can be readily obtained from the time derivative of Eq. (B23) by using Eq. (B19), $\partial_t\mathcal{F} = -\mathcal{R}F$, with Eq. (B16) and the permutation $\mathcal{B}_{j_n}\ldots\mathcal{B}_{j_{r+1}}\mathcal{C}_{j_r} = (-)^{n-r}\mathcal{C}_{j_r}\mathcal{B}_{j_n}\ldots\mathcal{B}_{j_{r+1}}$. We obtain

$$\begin{aligned}\partial_t \mathcal{F}_{\mathbf{j}}^{(n)} = &-\gamma_{\mathbf{j}}^{(n)}(t)\mathcal{F}_{\mathbf{j}}^{(n)} - i\sum_{r=1}^{n}(-)^{n-r}\mathcal{C}_{j_r}\mathcal{F}_{\mathbf{j}_r}^{(n-1)} \\ &- i\sum_{j;\sigma,s\in j}\mathcal{A}_s^{\bar\sigma}\mathcal{F}_{\mathbf{j}j}\end{aligned} \tag{B24}$$

with

$$\gamma_{\mathbf{j}}^{(n)}(t) = \sum_{r=1}^{n}\big[\tilde\gamma_{j_r} - \sigma_r i\Delta_{\alpha_r}(t)\big], \tag{B25}$$

which is just Eq. (10). While $\mathcal{F}_{\mathbf{j}}^{(n)}$ is the influence functional of the nth-tier ADO $\rho_{\mathbf{j}}^{(n)}$, where

$$\mathcal{F}_{\mathbf{j}_r}^{(n-1)} = \mathcal{B}_{j_n}\ldots\mathcal{B}_{j_{r+1}}\mathcal{B}_{j_{r-1}}\ldots\mathcal{B}_{j_1}\mathcal{F} \tag{B26}$$

and

$$\mathcal{F}_{\mathbf{j}j}^{(n+1)} = \mathcal{B}_j(\mathcal{B}_{j_n}\ldots\mathcal{B}_{j_1})\mathcal{F} \tag{B27}$$

are those of the $(n-1)$th-tier $\rho_{\mathbf{j}_r}^{(n-1)}$ and the $(n+1)$th-tier $\rho_{\mathbf{j}j}^{(n+1)}$, respectively. The HEOM (9) is simply the ADO's expression of Eq. (B24), while Eqs. (11) and (12) are the operator-level expressions of Eqs. (B5) and (B20), respectively, for the simplified case considered in Sec. II.

*yyan@ust.hk

[1] N. Agra, A. L. Yeyati, and J. M. van Ruitenbeek, Phys. Rep. **377**, 81 (2003).
[2] A. Pecchia and A. D. Carlo, Rep. Prog. Phys. **67**, 1497 (2004).
[3] N. Lorente, R. Rurali, and H. Tang, J. Phys.: Condens. Matter **17**, S1049 (2005).
[4] A. P. Horsfield, D. R. Bowler, H. Ness, C. G. Sánchez, T. N. Todorov, and A. J. Fisher, Rep. Prog. Phys. **69**, 1195 (2006).
[5] J. Kröger, Rep. Prog. Phys. **69**, 899 (2006).
[6] S. Roche, J. Jiang, L. E. F. Foa Torres, and R. Saito, J. Phys.: Condens. Matter **19**, 183203 (2007).
[7] M. Galperin, M. A. Ratner, A. Nitzan, and A. Troisi, Science **319**, 1056 (2008).
[8] M. Galperin, M. A. Ratner, and A. Nitzan, J. Phys.: Condens. Matter **19**, 103201 (2007).
[9] W. Ho, J. Chem. Phys. **117**, 11033 (2002).
[10] E. J. McEniry, T. N. Todorov, and D. Dundas, J. Phys.: Condens. Matter **21**, 195304 (2009).
[11] M. Galperin, K. Saito, A. V. Balatsky, and A. Nitzan, Phys. Rev. B **80**, 115427 (2009).
[12] R. Jorn and T. Seideman, J. Chem. Phys. **129**, 194703 (2008).
[13] A. V. Danilov, S. E. Kubatkin, S. G. Kafanov, K. Flensberg, and T. Bjønholm, Nano Lett. **6**, 2184 (2006).
[14] M.-L. Bocquet, H. Lesnard, and N. Lorente, Phys. Rev. Lett. **96**, 096101 (2006).

[15] J. Lambe and R. C. Jaklevic, Phys. Rev. **165**, 821 (1968).
[16] P. K. Hansma, Phys. Rep. **30**, 145 (1977).
[17] A. S. Alexandrov, A. M. Bratkovsky, and R. S. Williams, Phys. Rev. B **67**, 075301 (2003).
[18] A. S. Alexandrov and A. M. Bratkovsky, Phys. Rev. B **67**, 235312 (2003).
[19] S. Braig and K. Flensberg, Phys. Rev. B **68**, 205324 (2003).
[20] M. Galperin, M. A. Ratner, and A. Nitzan, J. Chem. Phys. **121**, 11965 (2004).
[21] M. Galperin, A. Nitzan, and M. A. Ratner, Phys. Rev. B **73**, 045314 (2006).
[22] T. Frederiksen, M. Paulsson, M. Brandbyge, and A. P. Jauho, Phys. Rev. B **75**, 205413 (2007).
[23] M. Paulsson, T. Frederiksen, and M. Brandbyge, Phys. Rev. B **72**, 201101 (2005).
[24] M. Paulsson, T. Frederiksen, H. Ueba, N. Lorente, and M. Brandbyge, Phys. Rev. Lett. **100**, 226604 (2008).
[25] S. Datta, *Electronic Transport in Mesoscopic Systems* (Oxford University Press, New York, 1995).
[26] H. Haug and A.-P. Jauho, *Quantum Kinetics in Transport and Optics of Semiconductors*, Springer Series in Solid-State Sciences, Vol. 123, 2nd ed. (Springer-Verlag, Berlin, 2008).
[27] J. Lehmann, S. Kohler, P. Hänggi, and A. Nitzan, Phys. Rev. Lett. **88**, 228305 (2002).
[28] X. Q. Li, J. Y. Luo, Y. G. Yang, P. Cui, and Y. J. Yan, Phys. Rev. B **71**, 205304 (2005).
[29] S. Welack, M. Schreiber, and U. Kleinekathöfer, J. Chem. Phys. **124**, 044712 (2006).
[30] U. Harbola, M. Esposito, and S. Mukamel, Phys. Rev. B **74**, 235309 (2006).
[31] X. Q. Li and Y. J. Yan, Phys. Rev. B **75**, 075114 (2007).
[32] P. Cui, X. Q. Li, J. S. Shao, and Y. J. Yan, Phys. Lett. A **357**, 449 (2006).
[33] H. Schoeller and G. Schön, Phys. Rev. B **50**, 18436 (1994).
[34] H. Schoeller and G. Schön, Physica B **203**, 423 (1994).
[35] J. König, H. Schoeller, and G. Schön, Europhys. Lett. **31**, 31 (1995).
[36] J. König, H. Schoeller, and G. Schön, Phys. Rev. Lett. **76**, 1715 (1996).
[37] J. S. Jin, X. Zheng, and Y. J. Yan, J. Chem. Phys. **128**, 234703 (2008).
[38] X. Zheng, J. S. Jin, and Y. J. Yan, J. Chem. Phys. **129**, 184112 (2008).
[39] X. Zheng, J. S. Jin, and Y. J. Yan, New J. Phys. **10**, 093016 (2008).
[40] X. Zheng, J. Y. Luo, J. S. Jin, and Y. J. Yan, J. Chem. Phys. **130**, 124508 (2009).
[41] X. Zheng, J. S. Jin, S. Welack, M. Luo, and Y. J. Yan, J. Chem. Phys. **130**, 164708 (2009).
[42] Y. Tanimura and R. Kubo, J. Phys. Soc. Jpn. **58**, 101 (1989).
[43] Y. Tanimura, Phys. Rev. A **41**, 6676 (1990).
[44] Y. Tanimura, J. Phys. Soc. Jpn. **75**, 082001 (2006).
[45] R. X. Xu, P. Cui, X. Q. Li, Y. Mo, and Y. J. Yan, J. Chem. Phys. **122**, 041103 (2005).
[46] R. X. Xu and Y. J. Yan, Phys. Rev. E **75**, 031107 (2007).
[47] J. S. Jin, S. Welack, J. Y. Luo, X.-Q. Li, P. Cui, R.-X. Xu, and Y. J. Yan, J. Chem. Phys. **126**, 134113 (2007).
[48] K. B. Zhu, R. X. Xu, H. Y. Zhang, J. Hu, and Y. J. Yan, J. Phys. Chem. B **115**, 5678 (2011).
[49] J. Xu, R. X. Xu, D. Abramavicius, H. D. Zhang, and Y. J. Yan, Chin. J. Chem. Phys. **24**, 497 (2011).
[50] J. J. Ding, J. Xu, J. Hu, R. X. Xu, and Y. J. Yan, J. Chem. Phys. **135**, 164107 (2011).
[51] J. S. Jin, X. Zheng, and Y. J. Yan, AIP Conf. Proc. **1074**, 96 (2008).
[52] R. P. Feynman and F. L. Vernon Jr., Ann. Phys. **24**, 118 (1963).
[53] H. Kleinert, *Path Integrals in Quantum Mechanics, Statistics, Polymer Physics, and Financial Markets*, 5th ed. (World Scientific, Singapore, 2009).
[54] J. Hu, R. X. Xu, and Y. J. Yan, J. Chem. Phys. **133**, 101106 (2010).
[55] J. Hu, M. Luo, F. Jiang, R. X. Xu, and Y. J. Yan, J. Chem. Phys. **134**, 244106 (2011).
[56] Y. Mo, X. Zheng, G. H. Chen, and Y. J. Yan, J. Phys.: Condens. Matter **21**, 355301 (2009).
[57] X. Zheng, G. H. Chen, Y. Mo, S. K. Koo, H. Tian, C. Y. Yam, and Y. J. Yan, J. Chem. Phys. **133**, 114101 (2010).
[58] A. Croy and U. Saalmann, Phys. Rev. B **80**, 245311 (2009).
[59] A. Fujiwara, Y. Takahashi, and K. Murase, Phys. Rev. Lett. **78**, 1532 (1997).
[60] H. Qin, A. W. Holleitner, K. Eberl, and R. H. Blick, Phys. Rev. B **64**, 241302 (2001).
[61] B. Dong, H. L. Cui, and X. L. Lei, Phys. Rev. B **69**, 205315 (2004).
[62] Y. S. Liu, H. Chen, X. H. Fan, and X. F. Yang, Phys. Rev. B **73**, 115310 (2006).
[63] J. Wang, X. Lu, and C. Q. Wu, J. Phys.: Condens. Matter **19**, 496216 (2007).
[64] L. H. Ryder, *Quantum Field Theory*, 2nd ed. (Cambridge University Press, Cambridge, 1996).